



CHORUS

This is the accepted manuscript made available via CHORUS. The article has been published as:

Observation of Flat Bands in Gated Semiconductor Artificial Graphene

Lingjie Du, Ziyu Liu, Shalom J. Wind, Vittorio Pellegrini, Ken W. West, Saeed Fallahi, Loren N. Pfeiffer, Michael J. Manfra, and Aron Pinczuk

Phys. Rev. Lett. **126**, 106402 — Published 12 March 2021

DOI: [10.1103/PhysRevLett.126.106402](https://doi.org/10.1103/PhysRevLett.126.106402)

1 **Observation of flat bands in gated semiconductor artificial** 2 **graphene**

3 **Lingjie Du^{1,2#*}, Ziyu Liu^{3#}, Shalom J. Wind², Vittorio Pellegrini⁴, Ken W. West⁵, Saeed**
4 **Fallahi⁶, Loren N. Pfeiffer⁵, Michael J. Manfra⁶, Aron Pinczuk^{2,3□}**

5 ¹ *School of Physics, and National Laboratory of Solid State Microstructures, Nanjing University, Nanjing 210093, China*

6 ² *Department of Applied Physics and Applied Mathematics, Columbia University, New York, New York 10027, USA*

7 ³ *Department of Physics, Columbia University, New York, New York 10027, USA*

8 ⁴ *Istituto Italiano di Tecnologia, Graphene Labs, Via Morego 30, I-16163 Genova, Italy.*

9 ⁵ *Department of Electrical Engineering, Princeton University, Princeton, New Jersey 08544, USA*

10 ⁶ *Department of Physics and Astronomy, and School of Materials Engineering, and School of Electrical and Computer Engineering,*
11 *Purdue University, IN, 47907, USA;*

12 [#]*L. J. □D. and Z. Y. L. contributed equally to this work*

13 ^{*}*ljdu@nju.edu.cn, □ap359@columbia.edu*

14
15 **Flat bands near M-points in the Brillouin zone are key features of honeycomb symmetry in**
16 **artificial graphene (AG) where electrons may condense into novel correlated phases. Here we**
17 **report the observation of van-Hove singularity doublet of AG in GaAs quantum well transistors,**
18 **which presents the evidence of flat bands in semiconductor AG. Two emerging peaks in**
19 **photoluminescence spectra tuned by back-gate voltages probe the singularity doublet of AG flat**
20 **bands, and demonstrate their accessibility to the Fermi level. As the Fermi level crosses the**
21 **doublet, the spectra display dramatic stability against electron density, indicating interplays**
22 **between electron-electron interactions and honeycomb symmetry. Our results provide a new**
23 **flexible platform to explore intriguing flat band physics.**

24
25
26 In two-dimensional electron systems (2DES), dispersion-less electron bands (flat bands)
27 present divergent density of states (DOS) (known as van-Hove singularity (VHS)). As the Fermi
28 level (E_F) crosses the VHS, electrons are usually unstable against the formation of new quantum
29 phases such as novel superconducting states and spin/charge density waves [1-3]. Nevertheless,
30 after extensive search, only limited electron structures have VHSs accessible for E_F . One famous
31 example is Landau levels in quantum Hall effect. Another is flat bands in ‘Moiré’ superlattices of
32 twisted atomic layers [4, 5], where superconductivity has been observed when E_F overlaps a flat
33 band of twisted-bilayer graphene [6]. In semiconductor artificial graphene (AG), pairs of flat
34 bands with honeycomb symmetry are predicted near the Brillouin zone (BZ) M-points [7-9].
35 Electron states in the semiconductor systems could be controlled by gating methods [10], giving
36 possibilities of bringing E_F to VHSs in semiconductor AG.

37
38 Semiconductor AG has electron band structures that could be tuned by honeycomb-lattice
39 periods [9, 11, 12]. Linearly dispersing Dirac bands have been observed in AG based on GaAs
40 quantum wells (QWs) [12]. Later the nanofabrication of antidots in AG provides a key element to
41 suppress impact of processing disorder on electrons [9]. However, probes of VHSs in the DOS of
42 semiconductor AG that are essential to confirm the presence of flat bands, have not been realized.

43 Scanning tunneling methods offered experimental accesses to VHSs in the DOS of twisted-bilayer
44 graphene [13] and to Dirac fermions in molecular AG [14], but are difficult to apply on
45 semiconductor AG buried under insulating layers. Optical emission (photoluminescence, PL)
46 could offer direct probes of the electron DOS in GaAs AG. PL spectra are from optical
47 recombination transitions between mobile electrons in conduction bands (CB) and weakly
48 photoexcited holes in valence bands (VB). Holes in GaAs AG have nearly dispersion-less VB so
49 that the lineshapes of PL spectra offer direct insights on the electron DOS [15-17]. The evolution
50 of PL spectra as a function of E_F , enabled by gating semiconductor AG, would distinguish
51 emerging optical characteristics.

52

53 In this letter we report the evidence of flat bands in carrier-density-dependent PL experiments
54 in semiconductor AG on a GaAs QW where the electron density n_e is tuned by a voltage V_b
55 applied to a back-gate fabricated in the device. PL spectra probe a striking emission doublet that
56 occurs when E_F crosses the flat band doublet in AG. The energy splitting of the characteristic PL
57 doublet is well described by the DOS singularities of flat bands near M-points. The carrier-density
58 dependence of the PL doublet further identifies it as the VHS doublet of flat bands. The
59 recombination energies and lineshapes of emission doublet remain constant over a wide range of
60 V_b , revealing remarkable interplay between Coulomb interactions and honeycomb symmetry of
61 electrons. The tunability of E_F to access flat bands would enable explorations of novel quantum
62 phases in nanofabricated semiconductor devices.

63

64 Figure 1(a) describes the back-gated AG device structure. A high-quality 2D electron gas is
65 confined in a 25nm single GaAs/ $\text{Al}_x\text{Ga}_{1-x}\text{As}$ QW modulation-doped with Si grown by molecular
66 beam epitaxy [10, 18]. The layer sequence and their composition have been optimized for optical
67 measurements. A n^+ $\text{Al}_x\text{Ga}_{1-x}\text{As}$ layer serves as a back-gate to tune n_e . As shown in Fig. 1(b), a
68 triangular-antidot lattice with period $a = 70$ nm (equivalent honeycomb-dot-lattice period $b = 35$
69 nm) is patterned on the QW by means of 80 keV e-beam lithography followed by reactive ion
70 etching [9, 19]. The AG lattice is on a mesa fabricated by wet-etching with phosphoric acid and
71 hydrogen peroxide. Ge/Pd/Au alloy-contacts are connected to the AG lattice and the back-gate.
72 The AG device is placed in an optical cryostat for measurements with a base temperature of 5 K.
73 Figure 1(d) shows calculated AG band structures with the device parameters, where a prominent
74 feature is a pair of flat bands around M-points. Figure 1(e) shows that the flat bands have VHSs
75 in the DOS in six equivalent valleys at M-points.

76

77 Figure 2(a) shows V_b dependence of PL spectra and Figure 2(b) describes
78 conduction-to-valence-band transitions active in the spectra. Holes in VB are subject to impact of
79 disorder, because their wavefunctions have maxima under antidots (green circles in Fig. 1(c)) [9].
80 Three regions of V_b are highlighted and their typical PL spectra are shown in Figs. 2(c)-2(e). The
81 Quasi-Uniform (QU) region (red in Fig. 2(a)) is for $V_b > 0.8$ V. PL spectra in this region are
82 dominated by a single broad peak Γ_0 at energies red-shifting with increasing V_b (see Fig. 2(c)).
83 The AG Quantum Limit (AL) region (green in Fig. 2(a)) is for -0.5 V $< V_b < 0.5$ V, which is
84 defined by the emergence of a strong PL doublet (M_0 and M_1) that is largely unchanged (see Fig.
85 2(d)). The Low-Density Limit (LDL) region (yellow in Fig. 2(a)) is for $V_b < -0.9$ V, where the PL
86 doublet finally merges into one main band (X) (see Fig. 2(e)).

87

88 Onset Γ_0 in the three regions is assigned to optical transitions from c_0 band electrons to VB
89 holes near Γ -point of the BZ. The broad PL band in region QU is similar to that from uniform
90 2DES in unpatterned QWs, whose lineshape yields an accurate estimation of E_F [15-17]. The
91 evaluation of E_F as a function of V_b in Fig. 3 estimates population changes of AG states. It shows
92 that at the start of region AL (0.5 V) E_F is near M_1 singularity and moves towards M_0 singularity at
93 $V_b < -0.1$ V. Remarkably, E_F always stays between the singularity doublet in region AL. This
94 implies that in region AL at 5 K optical transitions from the M_0 singularity make the largest
95 contribution to PL spectra.

96

97 At $V_b = 0.5$ V, n_e is estimated as $5.3 \times 10^{10} \text{ cm}^{-2}$ and E_F (~ 1.9 meV) is below the AG potential
98 5 meV [9]. Then electrons are largely confined in the red circles (unetched area in Fig. 1(b)) that
99 have honeycomb symmetry. In region AL the intensity step at 1518meV is continuously linked to
100 onset Γ_0 in region QU and thus attributed to optical recombination by electrons at the Γ -point (see
101 Fig. S1 of Supplemental Material [20]). Two peaks marked as M_0 and M_1 in Fig. 2(d) are the
102 strongest PL features in region AL. The lineshapes of PL spectra in region AL show significant
103 difference from ones in region QU and ones in the unpatterned QW (see Fig. S2 of Supplemental
104 Material [20]). Figure 2(d) shows that the doublet is also the strongest optical emission at 10 K,
105 which clearly reveals the presence of M_1 peak. The spectrum at 10 K is different from that at 5 K,
106 which could be linked to Coulomb interaction effects as we discuss below. Under higher
107 temperatures, electrons at Γ -point are thermally populated to higher levels, giving a lower
108 intensity of the Γ_0 -line. The doublet finally disappears above 20 K.

109

110 Remarkable changes in PL occur upon entering region AL where the Γ_0 -line is replaced by
111 the strong M_0 - M_1 doublet emission. This evolution of PL spectra can be interpreted as arising from
112 changes in the DOS when 2DES evolves from a quasi-uniform status in region QU to an AG
113 configuration in region AL where the DOS is given by honeycomb symmetry. The emergence of
114 M_0 - M_1 doublet in PL is continuous in the evolution from regions QU to AL (see Fig. S1 of
115 Supplemental Material [20]). The energy of the M_0 -line is 1 meV higher than that of the Γ_0 -line,
116 consistent with the situation that the singularity of the lower flat band is 1 meV higher than the CB
117 around Γ -point (see Fig. 1(e)). The energy separation between M_0 and M_1 peaks is about 0.9 meV,
118 close to that of VHSs (relevant optical transitions are shown in Fig. 2(b)). Thus, we could attribute
119 the M_0 - M_1 doublet to the VHS doublet of AG flat bands. The explanation of the doublet splitting is
120 supported by the density-functional study finding that key features of AG bands are stable against
121 electron-electron interactions [21]. The carrier-density-dependent PL experiments reveal emerging
122 VHSs and confirm the presence of AG flat bands. Previous RILS experiments [9, 12] that probe
123 joint DOS between AG bands suggest that the two AG bands near M-points are parallel, but
124 cannot encode the energy dispersion of each single flat band (see Fig. S3 of Supplemental
125 Material [20]).

126

127 The honeycomb symmetry of AG bands is linked to the constancy of doublet energies. As
128 shown in Figs. 2(a) and 4(a), the PL doublet energies don't change in region AL, which could be
129 interpreted in terms of the symmetry of the DOS singularity at M-points of the BZ where there are
130 six equivalent valleys sharing n_e . Figure 3 shows that n_e in region AL is typically about 4×10^{10}

131 cm^{-2} . We estimate that n_e in each valley of the M_0 singularity is tuned down by V_b from 2.3×10^9
132 cm^{-2} when states of the M_0 singularity are fully populated, to nearly full depletion when E_F is
133 below the singularity. This is a relatively small density variation that would not change the optical
134 recombination energy of electrons in GaAs QWs [22, 23].

135

136 The discussions above demonstrate that the energy properties of PL doublet can be captured
137 by the single-particle picture based on honeycomb symmetry. Nevertheless, detailed PL spectra
138 behaviors cannot be understood by single-particle physics. The lineshapes of PL spectra in region
139 AL cannot be described by calculations based on AG DOS. The intensity ratio of the M_0 -line over
140 the M_1 -line in experiments is lower than those in single-particle calculations (see Fig. S4 of
141 Supplemental Material [20]). Moreover, as shown in Fig. 4(a), the intensity of M_0 and M_1
142 transitions is fixed for $V_b > -0.1$ V, and their ratio is fixed across region AL. In a single-particle
143 picture, this behavior indicates that the population ratio between M_0 and M_1 singularities is fixed,
144 which is unlikely to happen because E_F sweeps from one singularity to another (see Fig. S5 of
145 Supplemental Material [20]).

146

147 Many-body interactions, including exchange interactions in the flat band doublet, would play
148 an important role in understanding detailed PL spectra behaviors. In region AL, E_F stays between
149 the singularity doublet (see Fig. 3), and the AG states are thus similar to those reported in Ref. [9],
150 where large exchange interactions between AG bands (the exchange energy is about 0.6 meV ≈ 8
151 K) were reported. We could get some insights about this physics process from the Coulomb
152 coupling between Fermi edge singularity and higher sub-band excitons [24-27]. Here the lower
153 flat band is heavily populated while the upper flat band is weakly populated by thermal excitations
154 and basically empty, thus the M_1 -line intensity should be low under single-particle physics.
155 However, the exchange energy between electrons in two flat bands is comparable with the
156 splitting of flat bands, and Coulomb coupling would provide extra scattering channels from the
157 lower flat band below E_F to the upper flat band. The strong coupling between the flat band doublet
158 would contribute to a considerable luminescence intensity to M_1 singularity, thus strengthens the
159 ratio of the M_1 -line intensity over the M_0 -line intensity.

160

161 On the other hand, due to honeycomb symmetry, each valley has a small n_e . Under the small
162 n_e born with the AG device, the Coulomb-interaction terms between the flat band doublet that are
163 dominated by exchange coupling processes should have weak dependence on n_e and V_b [22, 23].
164 Therefore, the doublet intensity is stable as long as the Coulomb coupling dominantly modifies the
165 luminescence intensity. The striking stability of PL spectral lineshapes in region AL suggests
166 many-body interactions interplayed with symmetry of AG electrons. This can be confirmed by PL
167 spectra under high temperatures. As shown in Fig. 2(d), for a higher temperature 10 K exceeding
168 the exchange energy, the PL spectral lineshape becomes unstable and the population ratio between
169 M_0 and M_1 singularities changes. The larger M_1 -line intensity at 10 K would be attributed to the
170 major effect of excitons from thermally elevated electrons into the upper flat band [24]. A detailed
171 lineshape analysis should consider evolution of localized states and is out of the scope of this
172 paper.

173

174 The Coulomb coupling would be modulated as E_F crosses the lower flat band for $V_b < -0.1$ V

175 (see Fig. 3). Figure 4(a) shows that the PL intensity starts to drop for $V_b < -0.1$ V, indicating the
176 beginning of depopulation of M_0 singularity (see insets of Fig. 4(a)). At $V_b < -0.9$ V, M_0 transition
177 quickly collapses and the doublet evolves into one broad band labeled X (Fig. 4(b)). The
178 contrasting lineshapes in regions LDL and AL indicate different underlying processes. At $V_b =$
179 -1.1 V, E_F is well below M_0 singularity and the population of M_0 - M_1 doublet is greatly reduced, so
180 optical transitions from these states can be considered as excitonic. Instead of a doublet, band X in
181 Fig. 4(b) indicates the mixture of excitonic transitions from each singularity by strong coupling
182 between the doublet [9]. The attribution of band X to excitons is consistent with significant
183 redshifts of its PL energies in region LDL (see Figs. 2(a) and 4(b)). The operation of V_b to reduce
184 n_e results in an increase of the electric field at the QW. Then, the redshift could be understood in
185 terms of a quantum-confined-Stark effect of excitons [28] that brings redshifts of about 0.5 meV
186 for electric field changes of 5×10^3 V/cm. We note that the appearance of excitonic transitions
187 above E_F is not trivial and implies couplings between the Fermi sea and higher AG bands [24, 25].
188

189 To summarize, flat bands are observed in carrier-density-dependent PL experiments in a
190 back-gated semiconductor AG device. PL spectra show striking dependence on carrier densities
191 tuned by V_b , marked by three regions with contrasting spectral lineshapes, and proves that the flat
192 bands of semiconductor AG are accessible by E_F . Under appropriate flat bands population,
193 Coulomb interactions within the flat band doublet are observed and take a critical role in stability
194 of PL spectra. Several key features of semiconductor AG make it an excellent platform for further
195 studies. For example, transport measurements could investigate many-body physics in the
196 embedded flat bands, e.g., unconventional superconductivity [2, 3, 29]. Under strong magnetic
197 fields [30], correlated phases such as Mott-Hubbard bands observed in honeycomb lattices [31]
198 could promise novel collective behaviors. In general, compared with 2D Moiré heterostructures,
199 AG can be employed as a seminal quantum simulator of electron correlation operating in a rarely
200 studied density regime.

201

202

203 Acknowledgement

204 The work at Columbia University was supported by the National Science Foundation,
205 Division of Materials Research under award DMR-1306976 and by grant DE-SC0010695 funded
206 by the US Department of Energy Office of Science, Division of Materials Sciences and
207 Engineering. Work at Nanjing University was supported by the Fundamental Research Funds for
208 the Central Universities (Grant No. 14380146) and National Natural Science Foundation of China
209 (Grant No. 12074177). This research is funded in part by the Gordon and Betty Moore
210 Foundation's EPiQS Initiative, Grant GBMF9615 to L. N. Pfeiffer, and by the National Science
211 Foundation MRSEC grant DMR 1420541. Work at Purdue University was supported by the U.S.
212 Department of Energy, Office of Science, Basic Energy Sciences, under Award DE-SC0006671.

213

214

215 References

- 216 1. J. González, Kohn-Luttinger superconductivity in graphene. *Phys. Rev. B* **78**,205431 (2008).
217 2. R. Nandkishore, L. S. Levitov and A. V. Chubukov, Chiral superconductivity from repulsive interactions in doped graphene,
218 *Nat. Phys.* **8**, 158 (2012).

219 3. R. Nandkishore, R. Thomale and A. Chubukov, Superconductivity from weak repulsion in hexagonal lattice systems. *Phys.*
220 *Rev. B* **89**, 144501 (2014).

221 4. R. Bistritzer and A. H. MacDonald, Moiré bands in twisted double-layer graphene, *Proc. Natl. Acad. Sci.* **108**, 12233 (2011).

222 5. Y. Cao, V. Fatemi, A. Demir, S. Fang, S. L. Tomarken, J. Luo, J. Sanchez-Yamagishi, K. Watanabe, T. Taniguchi, E. Kaxiras,
223 R. Ashoori and P. Jarillo-Herrero, Correlated insulator behaviour at half-filling in magic-angle graphene superlattices. *Nature*
224 **556**, 80 (2018).

225 6. Y. Cao, V. Fatemi, S. Fang, K. Watanabe, T. Taniguchi, E. Kaxiras and P. Jarillo-Herrero, Unconventional superconductivity
226 in magic-angle graphene superlattices, *Nature* **556**, 43 (2018).

227 7. C. H. Park and S. G. Louie, Making massless Dirac Fermions from a patterned two-dimensional electron gas. *Nano Lett.* **9**,
228 1793 (2009).

229 8. M. Gibertini, A. Singha, V. Pellegrini, M. Polini, G. Vignale, A. Pinczuk, L. N. Pfeiffer and K. W. West, Engineering artificial
230 graphene in a two-dimensional electron gas. *Phys. Rev. B* **79**, 241406 (2009).

231 9. L. Du, S. Wang, D. Scarabelli, L. N. Pfeiffer, K. W. West, S. Fallahi, G. C. Gardner, M. J. Manfra, V. Pellegrini, S. Wind and
232 A. Pinczuk, Emerging many-body effects in semiconductor artificial graphene with low disorder, *Nat. Com.*, **9**, 3299 (2018).

233 10. J. D. Watson, G. A. Csáthy and M. J. Manfra, Impact of Heterostructure Design on Transport Properties in the Second
234 Landau Level of In Situ Back-Gated Two-Dimensional Electron Gases, *Phys. Rev. Appl.* **3**, 064004 (2015).

235 11. S. Wang, D. Scarabelli, Y. Kuznetsova, S. Wind, A. Pinczuk, V. Pellegrini, M. J. Manfra, G. C. Gardner, L. N. Pfeiffer and K.
236 W. West, Observation of electron states of small period artificial graphene in nano-patterned GaAs quantum wells, *Appl. Phys.*
237 *Lett.* **109**, 113101 (2016).

238 12. S. Wang, D. Scarabelli, L. Du, Y. Kuznetsova, L. N. Pfeiffer, K. W. West, G. C. Gardner, M. J. Manfra, V. Pellegrini, S.
239 Wind and A. Pinczuk, Observation of Dirac bands in artificial graphene in small period nano-patterned GaAs quantum wells. *Nat.*
240 *Nano.* **13**, 29 (2017).

241 13. G. Li, A. Luican, J. M. B. Lopes dos Santos, A. H. Castro Neto, A. Reina, J. Kong and E. Y. Andrei, Observation of Van
242 Hove singularities in twisted graphene layers, *Nat. Phys.* **6**, 109 (2009).

243 14. K. K. Gomes, W. Mar, W. Ko, F. Guinea and H. C. Manoharan, Designer Dirac fermions and topological phases in molecular
244 graphene, *Nature* **483**, 306 (2012).

245 15. A. Pinczuk, J. Shah, R. C. Miller, A. C. Gossard and W. Wiegmann, Optical Processes of 2D Electron-plasma in
246 GaAs-(AlGa)As Heterostructures, *Solid State Commun.* **50**, 735 (1984).

247 16. D. Kamburov, K. W. Baldwin, K. W. West, S. Lyon, L. N. Pfeiffer and A. Pinczuk, Use of microluminescence as a
248 contactless measure of the 2D electron density in a GaAs quantum well, *Appl. Phys. Lett.* **110**, 262104 (2017).

249 17. Y. Chung, K. W. Baldwin, K. W. West, N. Haug, J. Wetering, M. Shayegan and L. N. Pfeiffer, Spatial Mapping of Local
250 Density Variations in Two-dimensional Electron Systems Using Scanning Photoluminescence. *Nano Lett.* **19**, 1908 (2019).

251 18. L. N. Pfeiffer, Private Communication (2018).

252 19. L. Nádorník, M. Orlita, N. A. Goncharuk, L. Smrčka, V. Novák, V. Jurka, K. Hruška, Z. Výborný, Z. R. Wasilewski, M.
253 Potemski and K. Výborný, From laterally modulated two-dimensional gas towards artificial graphene, *New J. Phys.* **14**, 053002
254 (2012).

255 20. See Supplemental Material at (URL will be inserted by publisher) for detailed PL spectra, comparison between PL and RILS,
256 and single-particle calculations.

257 21. E. Räsänen, C. A. Rozzi, S. Pittalis and G. Vignale, Electron-Electron Interactions in Artificial Graphene, *Phys. Rev. Lett.*
258 **108**, (2012).

259 22. G. E. W. Bauer and T. Ando, Many-body effects on luminescence spectrum of modulation-doped quantum wells, *Phys. Rev.*
260 *B* **31**, 8321 (1985).

261 23. C. Delalande, G. Bastard, J. Orgonasi, J. A. Brum, H. W. Liu, M. Voos, G. Weimann and W. Schlapp, Many-Body Effects in
262 a Modulation-Doped Semiconductor Quantum Well. *Phys. Rev. Lett.* **59**, 2690 (1987).

263 24. W. Chen, M. Fritze, A. V. Nurmikko, M. Hong and L. L. Chang, Fermi-edge singularities and enhanced magnetoexcitons in
264 the optical spectra of GaAs/(Ga,Al)As single quantum wells. *Phys. Rev. B* **43**, 14738 (1991).

265 25. W. Chen, M. Fritze, W. Walecki, A. V. Nurmikko, D. Ackley, J. M. Hong and L. L. Chang, Excitonic enhancement of the
266 Fermi-edge singularity in a dense two-dimensional electron gas. *Phys. Rev. B* **45**, 8464 (1992).

267 26. P. Hawrylak, Coupling of excitons with excitations of the Fermi sea in asymmetric quantum wells. *Phys. Rev. B* **44**, 6262
268 (1991).

269 27. The physics origin of the doublet reported in this paper is different from Refs. 24-26 and a complete theoretical treatment
270 should consider two Coulomb coupled flat bands with many body enhancements at a small electron density.

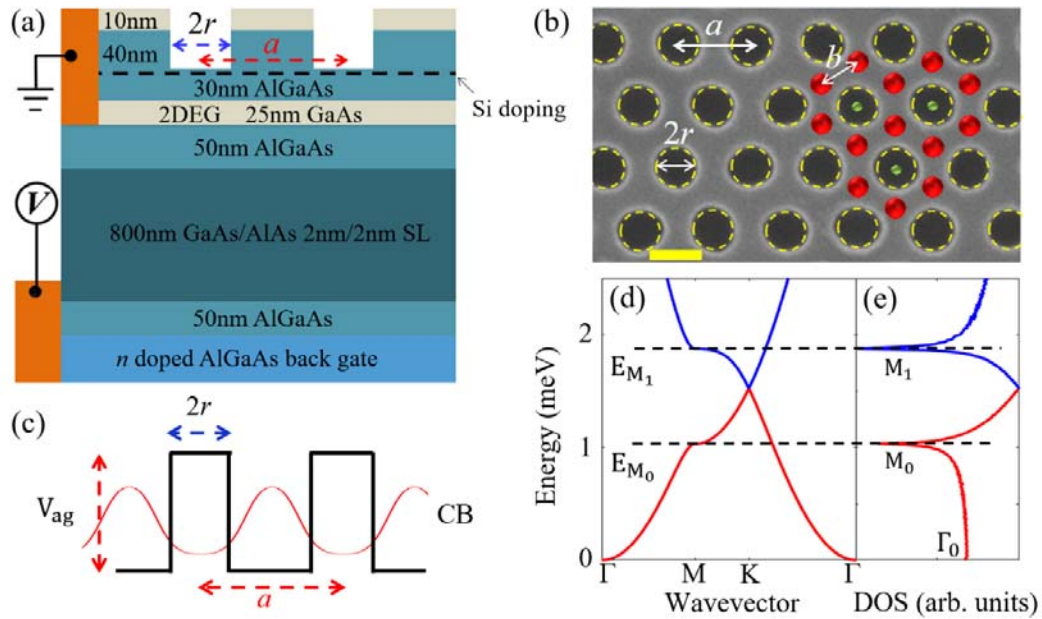
271 28. D. A. B. Miller, D. S. Chemla, T. C. Damen, A. C. Gossard, W. Wiegmann, T. H. Wood and C. A. Burrus, Band-Edge
272 Electroabsorption in Quantum Well Structures: The Quantum-Confined Stark Effect. *Phys. Rev. Lett.* **53**, 2173 (1984).

273 29. T. Li, J. Ingham and H. D. Scammell, arxiv.org/pdf/1909.07401(2019).

274 30. A. Patanè, N. Mori, O. Makarovskiy, L. Eaves, M. L. Zambrano, J. C. Arce, L. Dickinson and D. K. Maude, Manipulating and
275 Imaging the Shape of an Electronic Wave Function by Magnetotunneling Spectroscopy. *Phys. Rev. Lett.* **105**, 236804 (2010)

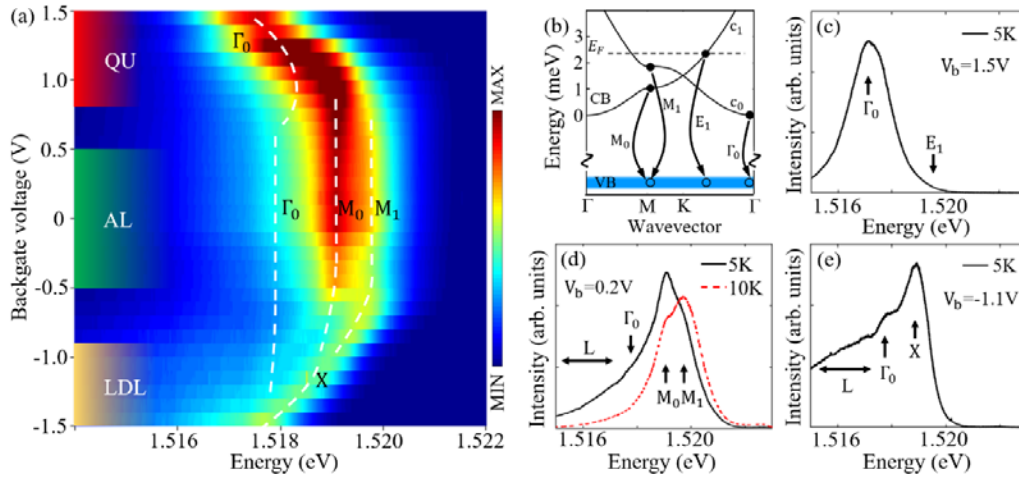
276 31. A. Singha, M. Gibertini, B. Karmakar, S. Yuan, M. Polini, G. Vignale, M. Katsnelson, A. Pinczuk, L.N. Pfeiffer, K.W. West
277 and V. Pellegrini, Two-dimensional Mott–Hubbard electrons in an artificial honeycomb lattice. *Science* **332**, 1176 (2011).

278
279
280
281
282
283
284
285
286
287
288
289
290
291
292
293
294
295
296
297
298
299
300
301
302



303
 304 Fig. 1 (color online). (a) Cross-section view of the AG device showing the heterostructure layer
 305 sequence with triangular antidot lattices imprinted on a GaAs QW. Dimensions are not to scale. The
 306 antidot radius is r and the period is a . (b) Scanning electron microscopy micrographs of AG lattices
 307 with $a = 70$ nm and $r = 20$ nm. The dashed circles mark antidots. The variation of r is below 5 nm. The
 308 scale bar is 50 nm. Red large dots indicate maximum positions of electron wavefunctions. Green small
 309 dots indicate positions of photoexcited holes. Holes are in a triangular lattice with a large effective
 310 mass, resulting in nearly dispersion-less VB. (c) Muffin-tin AG potential and wavefunctions in the
 311 single-particle approximation for electrons. (d) and (e) show the two lowest AG bands and DOS with
 312 the parameters in (b). In (e), the Γ -point onset, the singularity from a lower flat band and the singularity
 313 from an upper flat band are marked as Γ_0 , M_0 and M_1 . E_{M_1} and E_{M_0} mark energies of the upper and
 314 lower flat band.

315
 316
 317
 318
 319
 320
 321
 322
 323
 324
 325
 326
 327
 328



329

330

331 Fig. 2 (color online). (a) PL spectra as a function of V_b at 5 K. PL spectra were excited by tunable
 332 emissions from a Ti:Sapphire laser focused to a spot of $\sim 100 \mu\text{m}$ onto the AG device. Incident power
 333 was $3\text{-}10 \mu\text{W}$. Dashed lines mark PL peaks as Γ_0 , M_0 , M_1 and X. The color code is linear with intensity.
 334 (b) optical transitions in PL peaks between electron (dot) and hole (circle) states. E_1 represents the
 335 energy of transitions at E_F . The two lowest AG CBs are marked as c_0 and c_1 . (c) PL trace for $V_b = 1.5 \text{ V}$
 336 at 5 K. The difference between Γ_0 and E_1 yields a determination of E_F . (d) The black (dotted red) line
 337 represents PL trace under $V_b = 0.2 \text{ V}$ at 5 K (10 K). L indicates the transitions from localized states. (e)
 338 PL trace under $V_b = -1.1 \text{ V}$ at 5 K.

339

340

341

342

343

344

345

346

347

348

349

350

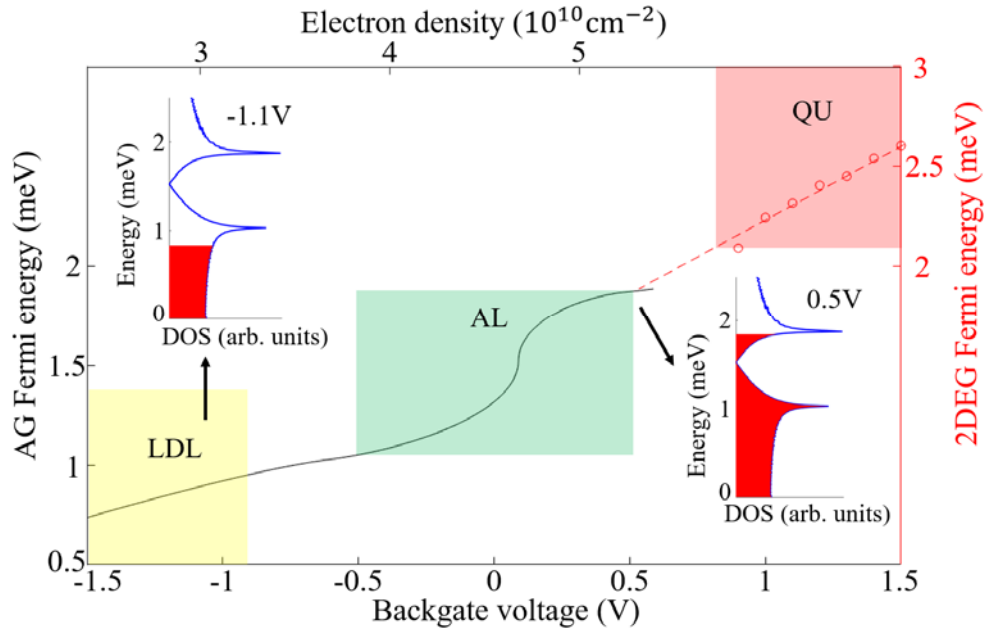
351

352

353

354

355



356

357

358

359

360

361

362

363

364

365

366

367

368

369

370

371

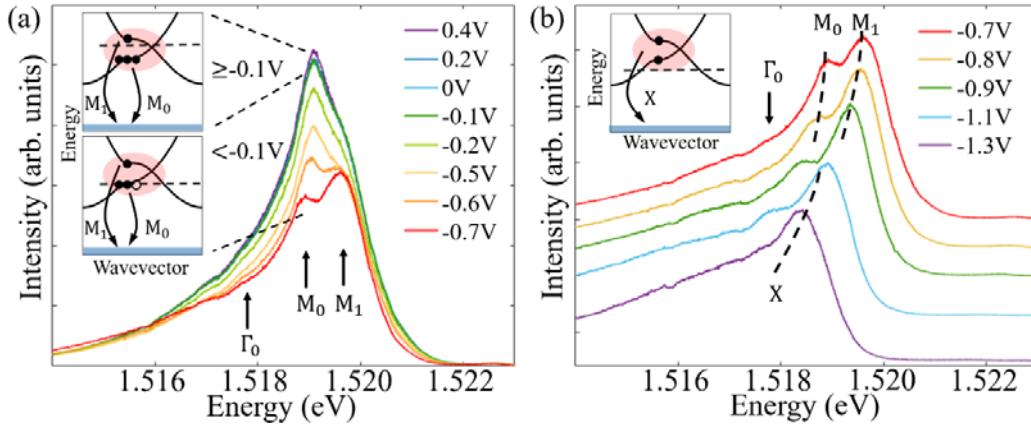
372

373

374

375

Fig. 3. (color online). E_F as a function of V_b (n_e). Red open circles and the red dashed line represent E_F determined from PL spectra and their linear extension. In region QU, E_F is transferred to n_e from difference between Γ_0 and E_1 as shown in Fig. 2(b) since electrons are quasi-two-dimensional. Because V_b tunes n_e linearly, it determines other n_e marked in the top axis. The black line represents the calculated E_F . Three regions in red, green and yellow are those defined in Fig. 2(a). Insets: schematic representations of AG band populations at $V_b = -1.1$ V and 0.5 V.



376
 377
 378
 379
 380
 381
 382
 383
 384
 385
 386
 387
 388
 389
 390
 391
 392

Fig. 4. (color online). (a) PL spectra in region AL. (b) PL spectra in the transition from AL to LDL regions. Insets: optical transitions at different voltage ranges. Filled and empty dots represent population changes in each flat band and the dashed red line marks E_F . The elliptical background denotes coupling between transitions. PL spectra of an unpatterned QW sharing the same contacts with the AG device show that its E_F is linear with V_b . In (b) at low n_e two excitonic transitions mix with each other and give a coupled excitonic transition (X). The large peak width comparable to the doublet energy splitting in (a) and (b), can be attributed to both thermal distribution of holes and electron-electron interactions. The lifetime broadening of electron states due to disorder is small (suggested by narrow inter-subband RILS peaks), and the peak width does not represent the sharpness of AG DOS.